Influence of ionic strength and carbonate on the Ca-P coating formation from SBF×5 solution

F. Barrere[a,b,*], C.A van Blitterswijk[a,b], K. de Groot[a,c], P. Layrolle[a]

[a] *IsoTis BV, PO Box 98, 3720 AB Bilthoven, The Netherlands*
[b] *Twente University, The Netherlands*
[c] *Leiden University, The Netherlands*

Abstract

Biomimetic calcium-phosphate (Ca-P) coatings were applied on Ti6Al4V by using simulated body fluids concentrated by a factor 5 (SBF×5). The production of SBF×5 solution was possible by decreasing the pH of the solution to approximately 6 using CO_2 gas. The subsequent release of this mildly acidic gas led to a pH rise and thus, increasing supersaturation. After immersion for $5\frac{1}{2}$ h a Ca-P coating on Ti6Al4V plates and a precipitate simultaneously formed at pH = 6.8. Sodium chloride (NaCl) and hydrogencarbonate (HCO_3^-) contents were studied in relation to CO_2 release and coating formation by changing their individual concentration in SBF×5 solution. On one hand, NaCl-free or low NaCl-content SBF×5 solution led to the earlier aspecific precipitation in the solution than for SBF×5 solution. In contrast, Ca-P coating was formed later and was thinner than the coating obtained in regular SBF×5 solution. High ionic strength delayed precipitation and favored Ca-P heterogeneous nucleation on Ti6Al4V. On the other hand, HCO_3^- content increased the pH of the solution due to its buffering capacity and influenced the release rate of dissolved CO_2. Thus, HCO_3^- content strongly affected the supersaturation and Ca-P structure. Furthermore, HCO_3^- favored the attachment of Ca-P mineral on Ti6Al4V by decreasing Ca-P crystal size resulting in a better physical attachment of Ca-P coating on Ti6Al4V substrate.
© 2002 Elsevier Science Ltd. All rights reserved.

Keywords: Biomimetic coating; Calcium-phosphate; Carbon dioxide; Carbonate; Ionic strength

1. Introduction

Titanium (Ti) and its alloys are widely used in orthopedic surgery because of their excellent mechanical properties that are required for load bearing applications like hip prostheses or dental plugs. These Ti implants are often coated with calcium-phosphate (Ca-P) coatings in order to enhance bone-bonding [1–8]. Furthermore, studies have shown that Ca-P crystals could nucleate easily on Ti and alloys in vitro [9–13] and in vivo [14–15] being thereby integrated into bone. In order to create Ca-P coatings onto Ti and alloys, different techniques have been developed [16–20]. Currently, hydroxylapatite (HA) coatings are deposited by plasma-spraying technique onto Ti substrate. Despite excellent clinical results [1–8], plasma-sprayed HA coatings have specific drawbacks related to the extre-

mely high processing temperatures and line of sight application. The biomimetic route is nowadays very promising for coating implants with Ca-P, overcoming plasma-spraying drawbacks. The biomimetic process consists at soaking implants under mild conditions of pH and temperature into simulated body fluid (SBF) solutions that have a similar inorganic content as human blood plasma [20]. Because of these physiological conditions, it is possible to coat heat-sensible materials such as polymers, and to cover complex shaped materials such as porous implants. Furthermore, this technique allows the covering of implants with new Ca-P phases [21–22] that could not be produced at high temperatures. These new biomimetic coatings have different structures and dissolution behavior depending on their crystal size and phase composition [23]. These specific characteristics could be highly beneficial for bone formation as compared with HA-plasma sprayed coating. However, the development of such biomimetic Ca-P coatings was limited by long immersion periods of

*Corresponding author. Fax: +31-030-228-0255.

E-mail address: florence.barrere@isotis.com (F. Barrere).

about 7–14 days with daily refreshments for achieving uniform Ca-P layers on various substrates [20,24–26]. Several studies have shown that chemical treatment of Ti surface could enhance the deposition of apatite-like layers [27–29]. Another possibility for shortening the coating process is by concentrating the SBF solution. However, SBF solutions are supersaturated at physiological pH and increasing the concentrations is limited by the low solubility of Ca-P. The idea of our work was thereby to increase the solubility of Ca-P phases by the use of a mildly acidic gas-like carbon dioxide (CO_2). Bubbling CO_2 allows the preparation of a stable five-times concentrated SBF (so-called SBF×5 solution). Once CO_2 supply is stopped, the gas is released out of the solution leading to an increase of pH and thus, to the formation of Ca-P salt in the solution and onto the Ti substrate [12]. In this work, we investigated the release kinetics of CO_2 in relation to SBF×5 composition and Ca-P coating formation. Since ionic strength or amphoteric ions are thought to affect gas solubility, we studied the influence of sodium chloride (NaCl) and hydrogencarbonate (HCO_3^-) contents on CO_2 release. Thereafter, we changed individually the concentration of either NaCl or HCO_3^- in relation to Ca-P formation in the soaking solution and onto Ti alloy (Ti6Al4V) samples.

2. Materials and methods

Several simulated body fluid solutions were prepared by changing salt concentrations as summarized in Table 1. All these solutions were derived from the classical SBF solution [20], in which ion concentrations were multiplied by five (SBF×5). Overall the experiments, the chemicals used for the study were reagents grade (Merck) precisely weighted. Each solution was prepared by dissolution of the salts into 1000 ml of demineralized water saturated with CO_2 gas at approximately 0.2 bar. The starting point of the experiments was set when CO_2

bubbling was stopped ($t = 0$ h). All the experiments were performed in a 1.5 l-reactor thermostated at $37 \pm 1°C$ with a soaking time of 24 h. The solutions were stirred with a magnetic bar at a speed of 200 rounds per minutes (rpm). The head plate of the reactor had open ports for a natural exchange of CO_2 with air.

2.1. Reference solutions

Prior to investigating the Ca-P coating formation into highly concentrated SBF solutions, the CO_2 release mechanism was studied in simple media (REF1, REF2, REF3 and REF4, see Table 1). The CO_2 release from a medium was expected to be influenced by HCO_3^- content and by ionic strength in the solution related to NaCl content. REF1 solution was simply composed of demineralized water. REF2 solution contained additionally $NaHCO_3$ salt in the same concentration than in SBF×5 solution. REF3 solution had a similar NaCl content than SBF×5. Finally, REF4 combines similar ionic strength and [HCO_3^-] than SBF×5. The pH of the REF solutions was recorded every 30 min for 24 h with a combined electrode (pH meter, Portamess). Prior to measurements, the pH electrode was calibrated at room temperature with two buffer solutions at pH = 4.01 and 7.00 (IUPAC standards, Radiometer Copenhagen).

2.2. Influence of the ionic composition of SBF solution on the Ca-P coating formation

Various highly concentrated SBF solutions (SBF×5) were prepared with different NaCl and HCO_3^- contents. SBF×5(NaCl×0) and SBF×5(NaCl×3) were, respectively, an NaCl-free solution and an NaCl-concentrated by three solutions. On the other hand, SBF×5(HCO3×0) was HCO3-free solution and SBF×5(HCO3×3) was a SBF×5 solution, where HCO_3^- content was reduced by three times. Besides HCO_3^- and NaCl contents, leftover salts, i.e. Mg^{2+}, Ca^{2+} and HPO_4^{2-} remained similar to SBF×5 (see Table 1). Twenty

Table 1
Inorganic composition (mM) of human blood plasma (HBP), regular simulated body fluid (SBF), reference (REF) solutions and experimental SBF solutions

	NaCl	$MgCl_2 \cdot 6H_2O$	$CaCl_2 \cdot 2H_2O$	$Na_2HPO_4 \cdot 2H_2O$	$NaHCO_3$
HBP	146.7	1.5	2.5	1.0	27.0
SBF	146.7	1.5	2.5	1.0	4.2
SBF×5	733.5	7.5	12.5	5.0	21.0
REF1	0.0	0.0	0.0	0.0	0.0
REF2	0.0	0.0	0.0	0.0	21.0
REF3	733.5	0.0	0.0	0.0	0.0
REF4	733.5	0.0	0.0	0.0	21.0
SBF×5(HCO3×0)	733.5	7.5	12.5	5.0	0.0
SBF×5(HCO3×3)	733.5	7.5	12.5	5.0	12.6
SBF×5(NaCl×0)	0.0	7.5	12.5	5.0	21.0
SBF×5(NaCl×3)	440.1	7.5	12.5	5.0	21.0

Ti6Al4V plates were soaked into each solution in order to investigate the coating formation mechanism.

Prior to the immersion, the Ti6Al4V plates were ultrasonically and successively cleaned into acetone, ethanol 70% and demineralized water for 15 min. These plates were then etched for 10 min by Kroll's reagent (a mixture of 2 ml HF (40%) and 4 ml HNO_3 (66%) in 1000 ml of water) in order to create a fresh titanium oxide (TiO_2) layer. The average roughness (R_a) of the substrate was not affected by etching and remained around $R_a = 0.80 \mu m$. The plates were individually and vertically fixed to polyethylene sample holders. Finally, Ti6Al4V plates were soaked into each solution at 37°C for 24 h, while pH was monitored.

A kinetic study was performed by measuring the pH of the solution, by taking out two Ti6Al4V plates every hour and by determining visually when the precipitation occurred in the solution. The pH of the solutions was recorded in the same conditions as the reference solutions. The removed Ti6Al4V plates were ultrasonically cleaned for 10 min in demineralized water in order to eliminate loose particles and to avoid late Ca-P formation. These samples were then dried overnight in air at 50°C. They were firstly observed macroscopically. Secondly, after carbon sputtering, these plates were then observed microscopically using Environmental Scanning Electronic Microscope equipped with a Field Emission Gun (ESEM, Philips, model XL-30, 15 keV). Energy dispersive for X-ray analysis (EDX, Philips) was performed to check the presence of any Ca-P coating (data not shown). All the precipitates formed during the experiments were filtrated through a Whatman paper no. 5 and dried as previously described. Thereafter, precipitates were characterized by Fourier transform infra-red spectroscopy (FTIR, 8 scans, Perkin-Elmer, Spectrum 1000) and by X-ray diffraction (XRD, Rigaku Miniflex goniometer). X-rays were produced by a monochromatic source (Cu K_α, $\lambda = 1.54 \text{Å}$, 30 kV, 15 mA). All the XRD patterns were recorded in the same conditions (scan range: $2\theta = 3.00–60.00°$, scan speed: $2.00°$/min, scan step: $0.02°$).

3. Results

3.1. Reference solutions

Fig. 1 exhibits the pH curves versus time for the various reference solutions. In the case of REF1 and REF3, the starting pH was rather similar, respectively, pH = 4.06 and 3.75, whereas in the case of REF2 and REF4, the starting pH was higher, respectively, pH = 6.29 and 5.99. This pH difference was due to the buffering capacity of HCO_3^-. Increasing HCO_3^- content resulted in higher initial and final pH values. Furthermore, the initial pH was slightly lower when the solution
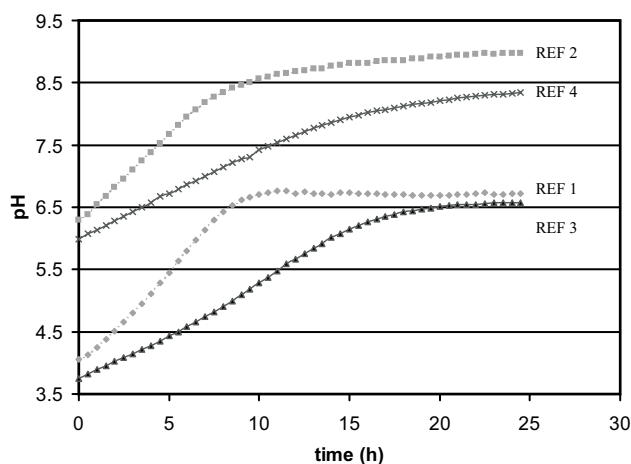

Fig. 1. pH profile versus time (h) for the various reference solutions: REF1 (a), REF2 (b), REF3 (c) and REF4 (d).

contained more NaCl. This indicated a slightly higher solubility of CO_2 gas for high ionic strength. For REF1 and REF2 solutions, the pH increased quickly with a rate of, respectively, 0.23 and 0.27 pH-units/h during the first 6 or 7 h. For REF3 and REF4 solutions, the pH increased slowly with an initial rate of, respectively, 0.15 and 0.145 pH-units/h. NaCl considerably affected the pH rise. After 7 h, the pH of REF1 solution reached a plateau at pH = 6.7 indicating that this solution reached an equilibrium state. In the case of REF2 solution, this plateau was also observed at approximately pH = 8.95 after 20 h. The pH of REF3 evolved even less rapidly at the end than at the beginning of the experiments. After 23 h, pH remained rather stable at pH = 6.55. Similarly, in the case of REF4 solution, pH increased less rapidly at the end of the experiment but did not remain stable. Depending on the HCO_3^- and NaCl contents, the pH evolution was different. This evolution was totally related to CO_2 gas release. Thereafter, it appeared that NaCl content, i.e ionic strength of the solution influenced the solubility of CO_2 gas while HCO_3^--content buffered the solutions.

3.2. Influence of the ionic composition of SBF solution on the Ca-P coating formation

All the results concerning the kinetic study and the Ca-P structures are summarized Table 2.

3.2.1. SBF×5: solution

As shown in Fig. 2a, the initial pH of SBF×5 solution was 6.2. During the overall experiment, the pH progressively increased to pH = 8.0 after 24 h. During the first 4 h, the pH increased with a slope of 0.11 pH-unit/h. Later on, the pH curve increased more slowly than at the beginning. Finally, after 24 h of soaking, the

Table 2
Kinetics of precipitation and coating formations of the various experiments

Experiment	Precipitation formation		Coating formation		Precipitate structure	Slope (/h)
	pH	Time (h)	pH	Time (h)		
SBF×5	6.7	$4\frac{1}{2}$	6.8	$5\frac{1}{2}$	$AmCO_3$–CaP	0.11
SBF×5(HCO$_3$×0)	6.2	18	6.2	18	DCPD	0.15
SBF×5(HCO$_3$×3)	6.8	$6\frac{1}{2}$	6.8	$6\frac{1}{2}$	$AmCO_3$–CaP	0.15
SBF×5(NaCl×0)	6.0	0	7.4	13	CO_3–Ap	0.21
SBF×5(NaCl×3)	6.8	$4\frac{1}{2}$	6.8	$4\frac{1}{2}$	$AmCO_3$–CaP	0.17
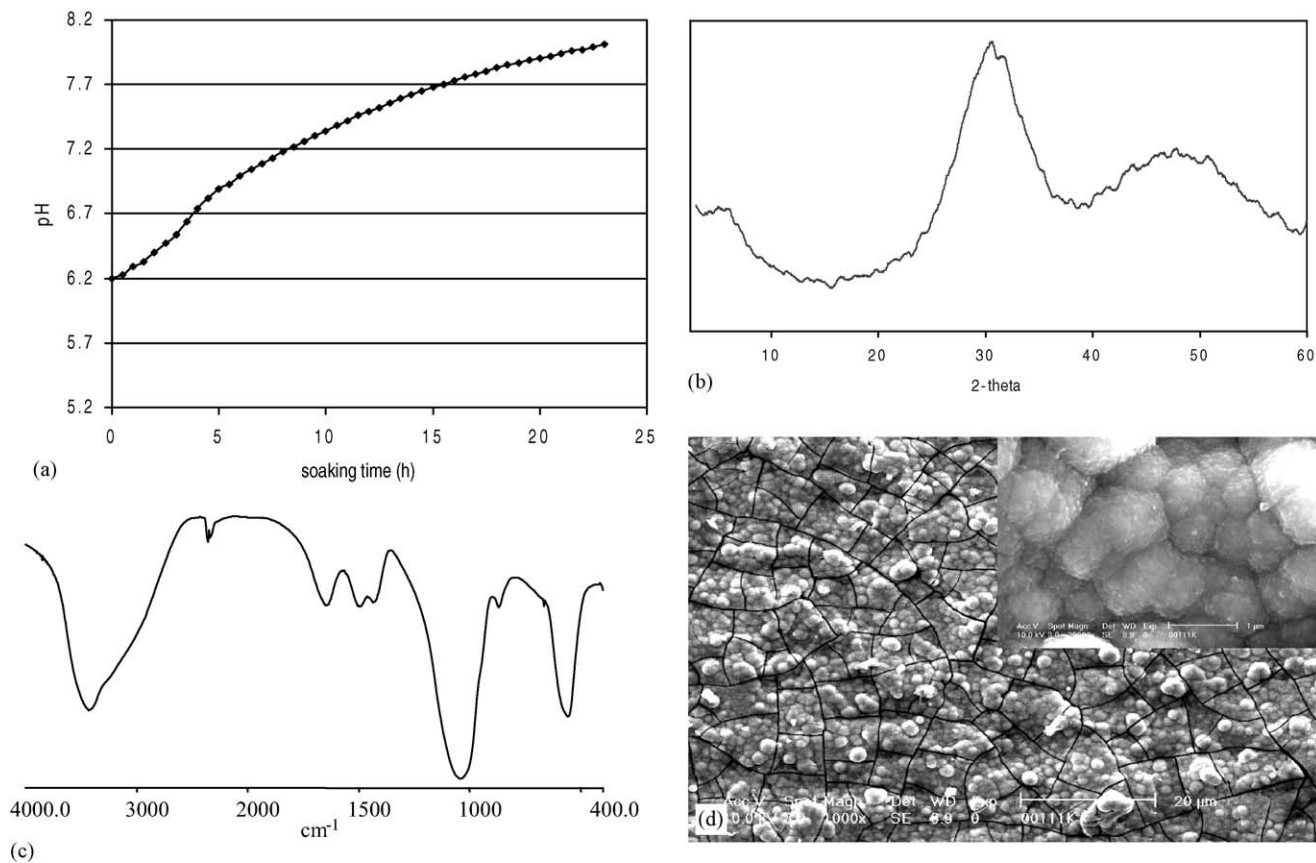
Fig. 2. SBF×5 experiment; (a) pH versus soaking time, (b) XRD, (c) FTIR, (d) ESEM photos at magnifications ×1000 and ×20000.

pH reached 8.0. At $t = 5\frac{1}{2}$ h, the solution became whitish: a precipitation occurred in the solution. The XRD pattern of the precipitate exhibited two wide bumps located at about $2\theta = 30°$ and at $2\theta = 45°$. These bumps are characteristic of the broadening of apatitic diffraction lines indicating a poorly crystallized structure (Fig. 2b). The FTIR spectrum corroborates the previous XRD observations. Intense and broad bands assigned to O–H stretching and bending of H_2O were observed at, respectively, 3435 and 1646 cm^{-1}. Additionally, three bands were assigned to CO_3^{2-} groups (v_3 mode at 1497 and 1428 cm^{-1} and v_2 mode at 868 cm^{-1}). The broad and one-component bands at 1043 and 560 cm^{-1} corresponded to the v_3 and v_4 P–O vibration modes of phosphate groups (PO_4^{3-}), while the band located at 868 cm^{-1} corresponded to P–(OH) stretching of HPO_4^{2-} groups. These featureless PO_4^{3-} bands were characteristic of a disordered environment. Therefore, the precipitate formed in SBF×5 is characteristic of a poorly crystallized or amorphous carbonated Ca-P phase $AmCO_3$–CaP. Simultaneous to the precipitation phenomenon, at $t = 5\frac{1}{2}$ h and pH = 6.8, a colorful layer appeared on the Ti6Al4V plates corresponding to a Ca-P layer. ESEM observations of the final coating after 24 h of immersion in SBF×5 indicated that the plate was covered by a uniform and dense Ca-P film composed of

globules of 1–5 μm in size (2d). At a high magnification (×20000), the globules exhibited nanometric spherical particles indicating that the film was composed of an amorphous or nanocrystalline apatite.

3.2.2. Influence of sodium chloride

In the case of NaCl-free solution (SBF×5(NaCl×0)), the starting pH value was 6.0. During approximately the first 2 h, the pH increased rapidly with a slope of 0.21 pH-units/h. Subsequently, pH remained stable for $1\frac{1}{2}$ h at pH = 6.25 and started to rise again. At the end of the experiment, pH of SBF×5(NaCl×0) solution reached 8.0 (Fig. 3a). A precipitation occurred immediately after adding the salts into SBF×5(NaCl×0) solution, thus at pH = 6.0. As shown in Fig. 3b, XRD pattern of this precipitate gathered at $t = 24$ h exhibits broad diffraction lines. The peak at $2\theta = 32.06°$ Corre-°Corresponded to the overlapping of (2 1 1), (1 1 2), (3 0 0) and (2 0 2) diffraction plans of apatitic structure. The FTIR spectrum of SBF×5(NaCl×0) precipitate (Fig. 3c) showed intense and broad bands assigned to O–H stretching and bending of H_2O (3435 and 1646 cm^{-1}), three bands corresponding to CO_3^{2-} groups (v_3 mode at 1497 and 1428 cm^{-1} and v_2 mode at 868 cm^{-1}). PO_4^{3-} groups were located at 1028 cm^{-1} (v_3 mode), at 960 cm^{-1} (v_1 mode) and at 602 and 563 cm^{-1} (v_4 mode). Furthermore, HPO_4^{2-} groups were detected at 1108 cm^{-1} (v_3 mode). This indicated a Ca-deficient carbonated apatitic structure. Thereby, SBF×5(NaCl×0) precipitate has a Ca-deficient carbonated apatitic structure. After 13 h of soaking, at pH = 7.4 a Ca-P film was detected by EDX on Ti6Al4V substrate. After 24 h of soaking, ESEM photos of the final coating showed that this layer was uniform and contained few globules smaller than 1 μm (Fig. 3d). Ti6Al4V texture was still visible beneath, indicating a very thin film. At high magnification (×20000), ESEM photos indicated that the substrate was uniformly coated with a Ca-P film. This film contained few cracks and it was composed of nano-sized Ca-P nuclei.

In the case of SBF×5(NaCl×3) solution ([NaCl] = 440 mM), the starting pH was pH = 6.1. During approximately the first 6 h, the pH increased rapidly with a slope of 0.17 pH-units/h (Fig. 3a). Subsequently, pH increased gradually. A precipitation in SBF×5(NaCl×3) solution occurred at $t = 4\frac{1}{2}$ h at pH = 6.8. XRD and FTIR spectra (respectively, Figs. 3b and c) of the final precipitate gathered at the end of the experiments indicated totally similar features than SBF×5 precipitate. In other words, the precipitate formed in SBF×5(NaCl×3) has an amorphous or nano-crystalline carbonated Ca-P structure. At $t = 6\frac{1}{2}$ h (pH = 6.8), a colorful Ca-P layer appeared on Ti6Al4V substrate. By ESEM, the final Ca-P layer was dense, though showing cracks, and it covered homogeneously the Ti6Al4V plate (Fig. 3d). The Ca-P coating was

composed of numerous Ca-P globules of 1–5 μm in diameter. At high magnification (×20000), the dense layer was composed of expanded globules containing nano-sized particles. No crystals could be detected. From these two experiments, we could see how NaCl content can affect the coating structure. Indeed, when ionic strength is high, it delays precipitation kinetics, allowing coating formation whereas for low ionic strength, precipitation occurs shortly leading to apatitic salts in the solution in detriment to the coating formation.

3.2.3. Influence of hydrogencarbonate

In the case of HCO_3-free solution SBF×5(HCO_3×0), the starting pH was pH = 5.3. During the first 10 h, the pH increased with a slope of 0.15 pH-units/h. Subsequently, the pH reached a plateau at $t = 10$ h for pH = 6.7. Suddenly at $t = 18$ h, the pH dropped until pH = 6.2 at the end of the experiment ($t = 24$ h) (Fig. 4a). A precipitation into SBF×5(HCO_3×0) solution started to occur at $t = 18$ h. XRD pattern of the precipitate gathered at the end of the experiments exhibited sharp peaks indicating a highly crystallized structure. The diffraction lines at $2\theta = 11.7°$ and at $2\theta = 29.3°$ are characteristic of a dicalcium phosphate dihydrate structure (DCPD, $CaHPO_4 \cdot 2H_2O$, Fig. 4b). FTIR spectrum confirmed previous XRD investigations that phosphate and hydrogenphosphate bands are characteristic of DCPD structure (1220, 1134 1074, 1059, 1000 and 986 cm^{-1} for $P-O$ v_3 mode, 874 cm^{-1} for $P-O(H)$ v_1 mode and 525 cm^{-1} for $P-O$ v_4 mode) (Fig. 4c). Tiny Ca-P crystals appeared on the Ti6Al4V surface at $t = 18$ h, simultaneously with the precipitation. After 24 h of soaking in SBF×5(HCO_3×0) solution, a whitish film covered approximately 50% of the Ti6Al4V surface. ESEM photos at magnification ×1000 showed that the Ti6Al4V plate was partially covered with tiny Ca-P crystals of approximately 1–2 μm in size (Fig. 4d). At high magnification (×20000), this layer seemed to be attached on some parts to the Ti6Al4V substrate. On other parts, the crystals seemed to lie on the surface without anchorage. This could suggest that the crystals were too large to remain attached on the Ti6Al4V substrate contrary to the small crystals that remained on the Ti6Al4V surface.

In the case of SBF×5(HCO_3×3) solution ([HCO_3] = 12.6 mM), the starting pH was pH = 5.9. During approximately the first 6 h, the pH increased rapidly with a slope of 0.15 pH-units/h. Subsequently, the pH increased more slowly than at the beginning. At $t = 24$ h, pH reached 7.6 (Fig. 4a). A precipitate formed into the solution at $t = 6\frac{1}{2}$ h (pH = 6.8). XRD and FTIR spectra (respectively, Figs. 4b and c) of the final precipitate gathered at the end of the experiments indicated totally similar features than SBF×5 and
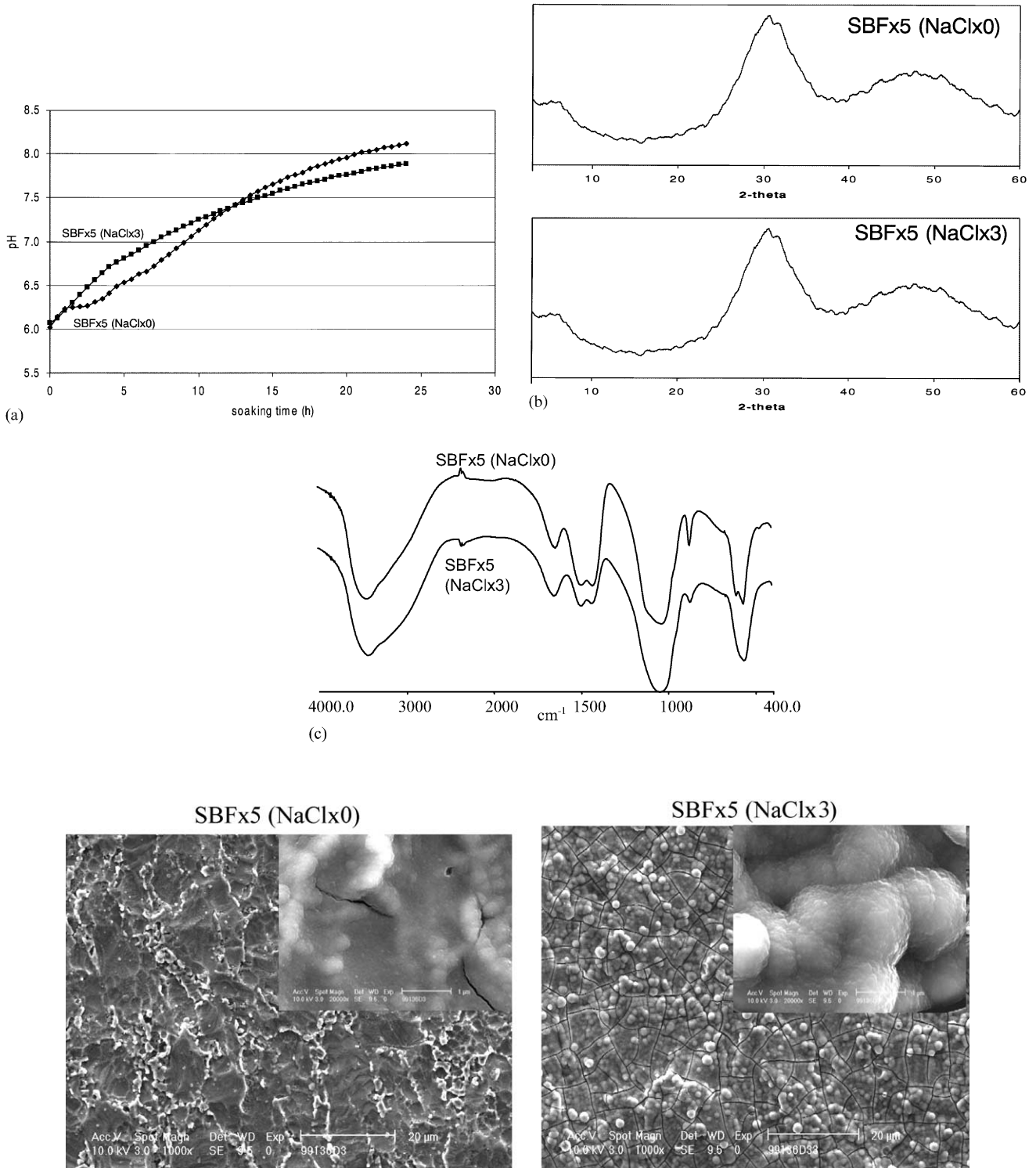
(a)

(b)

(c)

Fig. 3. SBF×5(NaCl×0) and SBF×5(NaCl×3) experiments; (a) pH versus soaking time, (b) XRD, (c) FTIR, (d) ESEM photos at magnifications ×1000 and ×20000.

SBF×5(NaCl×3) precipitates. In other words, the precipitate formed in SBF×5(HCO$_3$×3) has an amorphous or nano-crystalline carbonated Ca-P structure. At $t = 6\frac{1}{2}$ h (pH = 6.8), a colorful layer appeared on the substrate corresponding to the Ca-P coating as indicated by EDX. The ESEM observations of the final coating indicated that the coating was dense, though cracks, and uniformly composed of globules of 0.5–1 μm in diameter
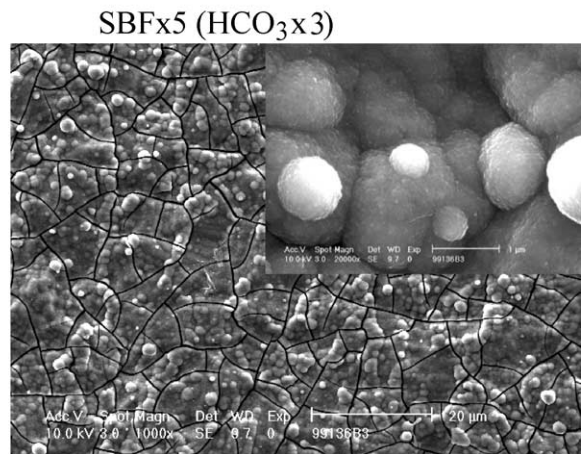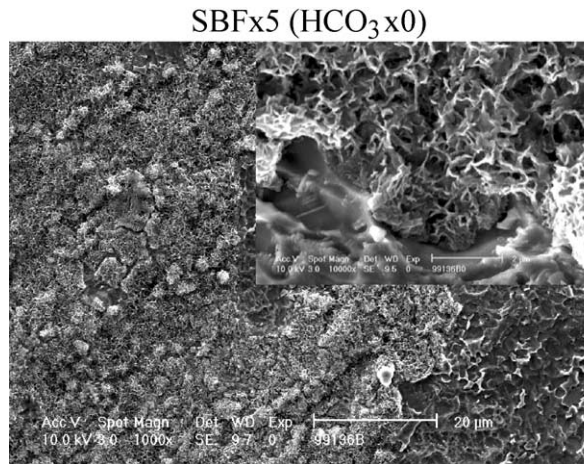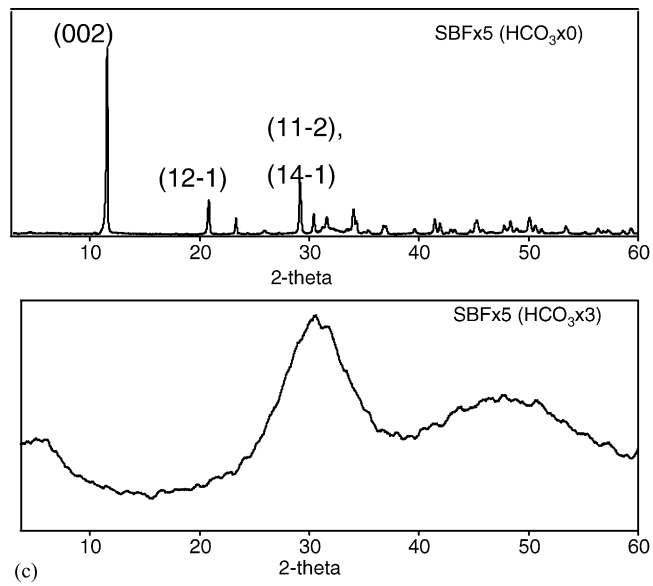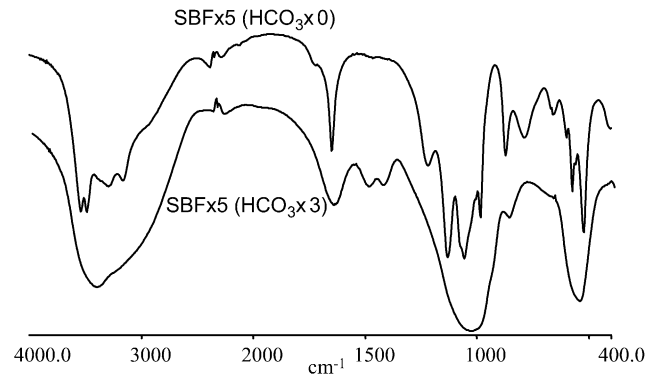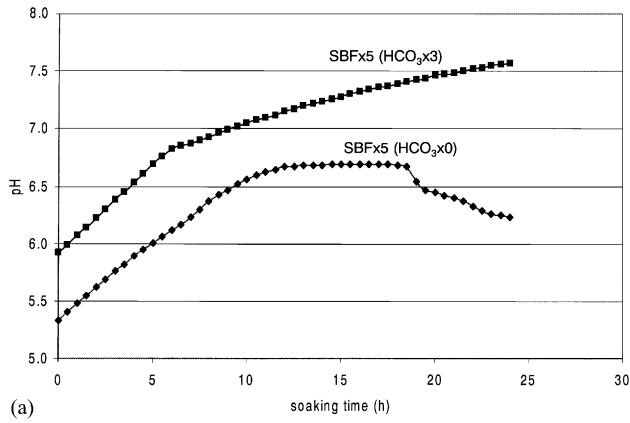
Fig. 4. Experiments SBF×5(HCO₃×0) and SBF×5(HCO₃×3), (a) pH versus soaking time, (b) XRD, (c) FTIR, (d) ESEM photos at magnifications ×1000 and ×20000.
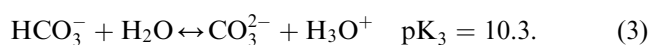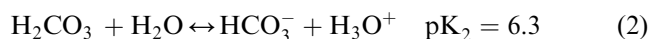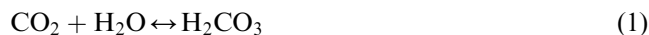
(Fig. 4d). At high magnification ($\times 20000$), the dense layer was composed of dense globules connected together. These globules were composed of nano-sized particles. No crystals were visible. From these two experiments, it is suggested that the size of the crystals, which formed on Ti6Al4V is critical for the homogeneity of the coating.

4. Discussion

The above experiments have demonstrated the possibility of producing Ca-P coatings on Ti6Al4V substrate within less than 24 h from highly concentrated SBF solutions. Visual observations reveal that the initial Ca-P film is colorful. This phenomenon is due to visible light diffraction by the coating thickness. Indeed, the coating is $< 1\,\mu m$ thick, i.e. nearly equal to visible light wavelength.

4.1. Effect of carbon dioxide supply into solutions

The stability of this highly concentrated solution (SBF$\times 5$) is due to the introduction of an acidic gas. It is very well known that the solubility of Ca-P salts increases with a decrease of pH [30]. Dissolution of CO_2 gas (solubility of 33.6 mmol/l at $25^\circ C$) leads to the formation of carbonic acid H_2CO_3 (reaction (1)). Immediately, this acid can be considered totally dissociated into HCO_3^- and CO_3^{2-} species (reactions (2) and (3)).

$$CO_2 + H_2O \leftrightarrow H_2CO_3 \qquad (1)$$

$$H_2CO_3 + H_2O \leftrightarrow HCO_3^- + H_3O^+ \quad pK_2 = 6.3 \qquad (2)$$

$$HCO_3^- + H_2O \leftrightarrow CO_3^{2-} + H_3O^+ \quad pK_3 = 10.3. \qquad (3)$$

Under these acidic conditions, it is possible to obtain stable highly concentrated solution like the SBF$\times 5$ solution. Once the CO_2 supply is stopped, the system returns to equilibrium by releasing dissolved CO_2 gas to air. The system, being open, tends to lower the pressure by releasing into the atmosphere. Thus, the gas release out of the solution leads to a slow and homogeneous pH increase following the left trend of relations (1), (2) and (3) as experimentally observed in the reference solutions REF1 to REF4. In the case of HCO$_3$-free reference solutions (REF1 and REF3), the final pH in the solution remains constant at about 6.7, indicating that all the CO_2 gas has been released. This final pH of the solution approaches that of pure water. In the case of HCO$_3$-containing reference solutions, the initial pH was higher than the HCO$_3$-free solutions due to the buffering effect of HCO_3^-/CO_3^{2-}. In the same way than for HCO$_3$-free reference solutions, the system returns to equilibrium by releasing CO_2 gas out of the solution. The equilibrium

pH for this system is set according to the equation applicable for conjugated weak acido-basic couples (4):

$$pH = 1/2(pK_2 + pK_3). \qquad (4)$$

In the case of H_2CO_3/HCO_3^- and HCO_3^-/CO_3^{2-} couples, the equilibrium pH is theoretically 8.3. The final pH values of the two carbonated reference solutions were slightly higher than this theoretical pH value. This might be due to an additional buffering effect of the amphoteric ion HPO_4^{2-}. In the case of the various SBF$\times 5$ solutions, the gas release induces a rise in pH. Progressively, the calcifying solutions reach their supersaturation point leading to Ca-P precipitation into the solution. Usually, Ca-P precipitation leads to a decrease of pH due to H^+ release according to the general reaction (5):

$$(10 - x)Ca^{2+} + 6HPO_4^{2-} + 2H_2O$$
$$\leftrightarrow Ca_{10-x}(HPO_4)_x(PO_4)_{6-x}(OH)_{2-x} + (6 - x)H^+. \quad (5)$$
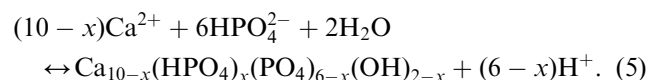
In our experiments, there is a combination of increase and decrease of pH due, respectively, to CO_2 release and Ca-P formation. The pH drop due to Ca-P precipitation was not always observed. This decrease in pH might be compensated by CO_2 release. However, a pH drop was observed for HCO$_3$-free SBF solution (SBF$\times 5$ (HCO$_3 \times 0$)). Two reasons can explain this phenomenon in this particular case. The absence of HCO_3^- reduces markedly a buffering capacity of SBF$\times 5$ solution, thus enhancing pH variations especially during Ca-P precipitation. Furthermore, HCO_3^- is known to reduce apatitic growth rate [31–33]. So in a HCO$_3$-free SBF$\times 5$ solution, apatite can precipitate more quickly leading to a sudden decrease in pH.

4.2. Study of Ca-P precipitation process

The precipitation indicates the stage when SBF$\times 5$ solutions reach saturation. From visual observations of precipitation in the various SBF$\times 5$ solutions, we can define three different groups. Firstly, in the case of NaCl-free solution, precipitation occurs immediately at the end of CO_2 supply at pH = 6.0. Secondly, precipitation occurs at pH = 6.8 in the case of low NaCl and HCO_3^- content solutions (SBF$\times 5$(NaCl$\times 3$) and SBF$\times 5$(HCO$_3^- \times 3$)) and in the case of the regular SBF$\times 5$ solution. Thirdly, in the case of HCO$_3$-free solution, precipitation occurs at pH = 6.2. So, NaCl and HCO_3^- contents affect precipitation kinetics and precipitate structure. Concerning NaCl influence, i.e. ionic strength, the reference solutions showed that CO_2 content is quite similar for high or low ionic strength. CO_2 is released at a faster rate at a low ionic strength. Thereby, at the starting point of the experiments, SBF$\times 5$(NaCl$\times 0$) solution fizzes to a larger extent than for all other calcifying solutions. In other words, with the lower ionic strength, more nucleation sites are

present in the solution. The increase in nucleation sites obviously enhances Ca-P precipitation in the solution. In addition, ionic diffusion is enhanced by low ionic strength favoring spontaneous precipitation even at a low pH value of 6.0. Interestingly, by comparing SBF$\times$5 and SBF$\times$5(NaCl$\times$0), despite their similar Mg^{2+} and HCO_3^- contents (well known as crystal growth inhibitors [31–35]), the precipitate appears more crystalline than the precipitate formed with a lower ionic strength than SBF$\times$5. Indeed, as we saw above, the ionic diffusion is enhanced by low ionic strength, so crystal growth is accelerated. It overcomes to a certain extent the inhibitory effect of HCO_3^- and Mg^{2+}. Concerning HCO_3^- content influence, a lack in HCO_3^- contents in the reference solutions leads to a lack of buffer capacity in the system. So the pH values in HCO_3-free solution are lower than the HCO_3-containing solutions. Under these mildly acidic conditions, this solution is supersaturated towards DCPD [36–37], which precipitates following reaction (5).

$$Ca^{2+} + H_2PO_4^{2-} + 3H_2O \rightarrow CaHPO_4 \cdot 2H_2O + H_3O^+$$

(5a)
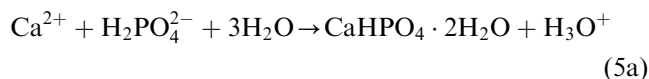
Additionally HCO_3^- species also have an inhibitory effect on Ca-P formation. It is difficult to compare the Ca-P precipitation kinetics versus $[HCO_3^-]$, because this concentration strongly affects the pH in the solution and thus the supersaturation. However, HCO_3^- inhibits apatite crystal growth in favor of poorly carbonated apatite. According to the position of CO_3^{2-} bands, CO_3^{2-} groups substitute PO_4^{3-} groups [38–39]. This carbonated apatite is the so-called type B substitution. This substitution leads to a distortion of the crystallographic lattice: *a*-axis contraction and *c*-axis extension. These distortions lead to a low crystallinity of apatite [31–33].

4.3. Study of Ca-P coating process

From the overall experiments, it can be conducted that Ca-P formed on Ti6Al4V substrate. These various Ca-P films are formed between $4\frac{1}{2}$ h and 18 h of immersion time. Thereby, this process is significantly accelerated as compared to regular supersaturated SBF solution buffered at pH = 7.4 [20, 24–26]. This fast deposition indicates that highly supersaturated calcifying solutions accelerate significantly the Ca-P coating formation on Ti6Al4V substrate. Like the precipitates, the coating deposition depends on the composition of the soaking solution. In the case of SBF$\times$5, SBF$\times$5 (HCO$_3\times$0), SBF$\times$5(HCO$_3\times$3) and SBF$\times$5(NaCl$\times$3), Ca-P coating forms simultaneously with the precipitation. So, the coating forms when the supersaturation in the solution is reached. In the case of SBF$\times$5(NaCl$\times$0) experiment, due to a low ionic strength, Ca-P coating forms on Ti6Al4V substrate later than precipitation in

the solution. This early and sudden precipitation lowers markedly the supersaturation of the solution. Thereby, less ionic species are available in the solution for the Ca-P nucleation on Ti6Al4V. Furthermore, there is a competition between the early formed Ca-P salt acting as seed and, heterogeneous nucleation on Ti6Al4V surface. When Ca-P forms very fast in the solution, the competition is detrimental to the coating formation. This explains the thin Ca-P coating obtained after 24 h of soaking in NaCl-free solution. Therefore, Ca-P coating formation on Ti6Al4V depends on the precipitation kinetics throughout the soaking in SBF$\times$5 solution. If the precipitate appears early in the solution, then it delays the coating formation process due to a low remaining supersaturation. Additionally, the amount of HCO_3^- into SBF$\times$5 solution influences Ca-P coating structure. The heterogeneity and the crystal size of the coating formed from SBF$\times$5(HCO$_3\times$0) suggest that Ca-P crystal size is also critical for coating stability. When Ca-P crystals are small, they remain well adhered onto the substrate, whereas when the layer is composed of large crystals, the Ca-P layer detaches from the Ti6Al4V substrate. Indeed, loading forces are greater for large and vertical crystals than for tiny Ca-P globules fixed into substrate cavities. It appears that HCO_3^- contributes efficiently to control the Ca-P crystal size due to apatite crystal distortion and, therefore physical attachment of Ca-P coating onto Ti6Al4V substrate.

5. Conclusion

The use of a mildly acidic gas CO_2 in a highly concentrated simulated body fluid solution allowed the formation of a Ca-P coating on Ti6Al4V within less than 24 h. This biomimetic method avoids particular surface treatment for Ti and refreshing of metastable SBF solutions. The coating deposition kinetics is influenced by the ionic strength of the solution and HCO_3^- content. NaCl controls the ionic strength of the solution and thereby, it controls CO_2 release, i.e. pH profile. Furthermore, ionic strength delays Ca-P precipitation in SBF$\times$5 solution allowing Ca-P to nucleate on Ti6Al4V. HCO_3^- acts as a buffer with the dissolved CO_2 gas. Furthermore, HCO_3^- reduces apatite crystal size of the coating allowing a better physical attachment on Ti6Al4V substrate. From these experiments, two important parameters can be highlighted on the biomimetic Ca-P formation process from SBF$\times$5 solutions. Firstly, precipitation in the solution must be delayed in order to favor heterogeneous nucleation on Ti6Al4V. Secondly, Ca-P particles deposited on the substrate must be nano-sized to remain physically attached on Ti6Al4V.

References

[1] Bauer TW, Geesink RCT, Zimmerman R, McMahon JT. Hydroxylapatite-coated femoral stems: histological analysis of components retrieved at autopsy. J Bone Jt Surg 1991;73: 1439–52.

[2] Geesink RGT. Hydroxyalapatite-coated hip implants: five year clinical and radiological results in hydroxylapatite coatings. In: Geesink RGT, Manley MT, editors. Orthopedic surgery. New York, US: Raven Press, 1993.

[3] Clemens JAM, Klein CPAT, Vriesde RC, Rozing PM, de Groot K. Healing of large (2 mm) gaps around calcium-phosphate coated bone implants: a study in goats with a follow-up of 6 months. J Biomed Mater Res 1998;40:341–9.

[4] Moroni A, Aspenberg P, Toksvig-Larsen S, Falzarano G, Giannini S. Enfanced fixation with hydroxyapatite coated pins. Clin Orthop 1998;346:171–7.

[5] Kroon PO, Freeman MA. Hydroxyapatite coating of hip prostheses. Effect on migration into the femur. J Bone Jt Surg Br 1992;74:518–22.

[6] Frayssinet P, Hardy D, Rouquet N, Giammara B, Guilhem A, Hanker J. New observations on middle term hydroxyapatite-coated titanium alloy hip prosthesis. Biomaterials 1992;13:668–74.

[7] Furlong RJ, Osborn JF. Fixation of hip prosthesis by hydroxyapatite ceramic coating. J Bone Jt Surg Br 1991;73:741–5.

[8] Soballe K, Toksvig-Larsen S, Gelineck J, Fruensgaard S, Hansen ES, Ryd L, Lucht U, Bunger C. Migration of hydroxyapatite coated femoral prostheses. A Roentgen stereophotogrammetric study. J Bone Jt Surg Br 1993;75:681–7.

[9] Combes C, Rey C, Freche M. XPS and IR study of dicalcium phosphate dihydrate nucleation on titanium surfaces. Colloid Surfaces B: Biointerfaces 1998;11:15–27.

[10] Li P. In vitro and in vivo calcium phosphate induction on gel oxide. PhD thesis, Leiden University, 1993.

[11] Healy KE, Ducheyne P. Hydration and preferential molecular adsorption on titanium in vitro. Biomaterials 1992;13:553–61.

[12] Barrere F, Layrolle P, van Blitterswijk CA, de Groot K. Fast formation of Ca–P coating on Ti6Al4V. Mater Res Soc Symp Proc 2000;599:135–40.

[13] Ong JL, Lucas LC. Auger electron spectroscopy and its use for characterization of titanium and hydroxyapatite surface. Biomaterials 1998;19:455–64.

[14] Hanawa T. Titanium and its oxide film: a substrate for formation of apatite. Davies JE editor. The bone-biomaterial interface, University Toronto Press, 1990. p. 49–61.

[15] Yan WQ, Nakamura T, Kobayashi M, Kim HM, Miyaji F, Kokubo T. Bonding of chemically treated titanium implants to bone. J Biomed Mater Res 1997;37:267–75.

[16] de Groot K, Geesink RGT, Klein CPAT, Serekian P. Plasma-sprayed coatings of hydroxylapatite. J Biomed Mater Res 1987;21:1375–81.

[17] Jansen JA, Wolke JGC, Swann S, van der Waerden JVPM, de Groot K. Application of magnetron sputtering for the producing ceramic coating on implant materials. Clini Oral Implant Res 1994;28:1477–84.

[18] Ducheyne P, Radin S, Heughebaert M, Heughebaert JC. Calcium phosphate ceramic coating on porous titanium: effect: effect of structure and composition on electrophoretic deposition, vacuum sintering and in vitro dissolution. Biomaterials 1990;11:244–54.

[19] Sardin G, Varela M, Morenza JL. Deposition of hydroxyapatite coatings laser ablation. In: Brown PW, Constanz B, editors. Hydroxyapatite and related materials. London: CRC press, 1994. p. 225–30.

[20] Kokubo T, Kushitani H, Sakka S, Kitsugi T, Yamamuro T. Solutions able to reproduce in vivo surface-structure changes in bioactive glass-ceramics A–W^3. J Biomed Mater Res 1990;24: 721–34.

[21] Barrere F, Layrolle P, van Blitterswijk CA, de Groot K. Biomimetic coatings on titanium: a crystal growth study of octacalcium phosphate. J Mater Sci: Mater Med 2001;12:529–34.

[22] Barrere F, Layrolle P, van Blitterswijk CA, de Groot K. Biomimetic Ca-P coating on Ti6Al4V: crystal growth study of octacalcium phosphate and inhibition by Mg^{2+} and HCO_3^-. Bone 1999;25:107S–11S.

[23] Barrere F, Stigter M, Layrolle P, van Blitterswijk CA, de Groot K. In vitro dissolution of various calcium-phosphate coatings on Ti6Al4V. Bioceramics 2001;13:67–70.

[24] Li P, Kangasniemi I, de Groot K, Kokubo T. Bonelike hydroxyapatite induction by a gel-derived titania on a titanium substrate. J Am Ceram Soc 1994;77:1307–12.

[25] Peltola T, Patsi M, Rahiala H, Kangasniemi I, Yli-Urpo A. Calcium phosphate induction by sol–gel-derived titania coatings on titanium substrates in vitro. J Biomed Mater Res 1998;41:504–10.

[26] Li P, Ducheyne P. Quasi-biological apatite film induced by titanium in a simulated body fluid. J Biomed Mater Res 1998;41:341–8.

[27] Wen HB, Wolke JGC, de Wijn JR, Cui FZ, de Groot K. Fast precipitation of calcium phosphate layers on titanium induced by simple chemical treatment. Biomaterials 1997;18:1417–78.

[28] Ohtsuki C, Iida H, Hayakawa S, Osaka A. Bioactivity of titanium treated with hydrogen peroxide solutions containing metal chloride. J Biomed Mater Res 1997;35:39–47.

[29] Kim HM, Miyaji F, Kokubo T, Nakamura T. Preparation of bioactive Ti and its alloys via simple chemical surface treatment. J Biomed Mater Res 1996;32:409–17.

[30] Elliot JC. Structure and chemistry of the apatites and other calcium orthophosphates, Amsterdam, The Netherlands: Elsevier, 1994.

[31] Barralet J, Best S, Bonfield W. Carbonate substitution in precipitated hydroxyapatite: an investigation into the effects of reaction temperature and bicarbonate concentration. J Biomed Mater Res 1998;41:79–86.

[32] Chikerur NS, Tung MS, Brown WE. A mechanism for incorporation of carbonate into apatite. Calcif Tissue Int 1980;32:55–62.

[33] Newesely H. Changes in crystal types of low solubility calcium phosphates in the presence of accompanying ions. Arch Oral Biol (Special Suppl) 1961;6:174–80.

[34] Tomazic B, Tomson M, Nancollas GH. Growth of calcium phosphates on hydroxyapatite crystals: the effect of magnesium. Arch Oral Biol 1975;20:803–8.

[35] Salimi MH, Heughebaert JC, Nancollas GH. Crystal growth of calcium phosphates in the presence of magnesium ions. Langmuir 1985;1:119–22.

[36] Combes C, Freche M, Rey C. Nucleation and crystal growth of dicalcium phosphate dihydrate on titanium powder. J Mater Sci: Mater Medicine 1995;6:699–702.

[37] de Rooij JF, Heughebaert JC, Nancollas GH. A pH study of calcium phosphate seeded precipitation. J Colloid Interface Sci 1984;100:350–8.

[38] Heughebaert JC. Contribution a l'etude de l'evolution des orthophosphates de calcium precipites amorphes en orthophosphates apatitiques. These d'Etat INP Toulouse, 1977.

[39] Nelson DGA, Featherstone JDB. Preparation, analysis and characterization of carbonated apatites, calcif. Tissue Int 1982;34:SS69.